

Chapter 2

Topological Invariant and Topological Phases

2.1 Integer Quantum Hall Effect

Historically in two-dimensional electron gas (2DEG) subjected to a strong magnetic field, the integer quantum Hall (QH) effect was observed experimentally for the first time by von Klitzing et al. [1]. In the QH effect, the Hall conductivity is given as $\nu \frac{e^2}{h}$ where ν is an integer. The quantized Hall conductivity was interpreted in terms of gauge invariance [2, 3] under flux insertion and later topological invariance was proposed [4] to interpret its physical origin. Here we explain the topological number ν given by Thouless, Kohmoto, Nightingale and den Nijs (TKNN) [4]. This ν number is called the TKNN number and was calculated from the Kubo formula at first. Later it was found to be interpreted as the Chern number given by an integral of the Berry curvature [5], as we explain in the following.

In quantum mechanics, when quantum states are subjected to an adiabatic transition, the Berry connection (phase) appears as a change of the phase of the wavefunction. In addition, the Hall current by the Kubo formula have the same form with this phase change. Besides the Kubo formula, the Hall current contributed from the Berry curvature can also be calculated from the Schrödinger equation as follows [6]. We consider a time-dependent 2D system with translational symmetry along the x and y axes. The Hamiltonian is written as $H(\mathbf{k}(t))$, where $\mathbf{k} = (k_x(t), k_y(t))$ is the wavevector, and the eigenstate and eigenvalue are $|u_{\mathbf{k}}\rangle$ and $E_{\mathbf{k}}$, respectively. The current along the x axis $I_x(\mathbf{k})$ is expressed as

$$\begin{aligned} I_x &\sim \left\langle u_{\mathbf{k}} \left| \frac{\partial H(\mathbf{k}(t))}{\partial k_x} \right| u_{\mathbf{k}} \right\rangle \\ &= \partial_x E_{\mathbf{k}} - \langle \partial_x u_{\mathbf{k}} | H(\mathbf{k}) | u_{\mathbf{k}} \rangle - \langle u_{\mathbf{k}} | H(\mathbf{k}) | \partial_x u_{\mathbf{k}} \rangle, \end{aligned} \quad (2.1)$$

where $\partial_x = \frac{\partial}{\partial k_x}$. Then by the Schrödinger equation,

$$H(\mathbf{k})|u_{\mathbf{k}}\rangle = i \frac{\partial}{\partial t} |u_{\mathbf{k}}\rangle = i(\dot{k}_x \partial_x + \dot{k}_y \partial_y) |u_{\mathbf{k}}\rangle, \quad (2.2)$$

we have

$$I_x(\mathbf{k}) \sim \partial_x E_{\mathbf{k}} - b_z(\mathbf{k})\dot{k}_y, \quad (2.3)$$

$$b_z(\mathbf{k}) = i(\langle \partial_x u_{\mathbf{k}} | \partial_y u_{\mathbf{k}} \rangle - \langle \partial_y u_{\mathbf{k}} | \partial_x u_{\mathbf{k}} \rangle). \quad (2.4)$$

The quantity $b_z(\mathbf{k})$ defined in Eq. (2.4) is called the Berry curvature. The first term $\partial_x E_{\mathbf{k}}$ in Eq. (2.3) corresponds to the velocity along the x axis. For the second term in Eq. (2.3), when an electric field \mathbf{E} is applied along the y axis, the temporal differential of the wavenumber corresponds to the electronic field $\dot{k}_y \sim -\frac{eE_y}{\hbar}$, and the Hall conductivity is given as the Berry curvature $\sigma_{xy} \sim b_z(\mathbf{k})$. Therefore we have shown that the Berry curvature contributes to the Hall current. Furthermore,¹ when the system is gapped, the contribution from one of the occupied band to σ_{xy} is given by the sum of the Berry curvature over the Brillouin zone (BZ) as,

$$\sigma_{xy} = v \frac{e^2}{h}, \quad (2.5)$$

$$v = \frac{1}{2\pi} \int_{\text{BZ}} d^2k b_z(\mathbf{k}), \quad (2.6)$$

where v is an integer (see Sect. 6.1). This is the TKNN integer, also called the Chern number.

By extending the above discussion to general band structure, the Hall conductivity is expressed as

$$\sigma_{xy} = v \frac{e^2}{h}, \quad (2.7)$$

$$\begin{aligned} v &= \frac{i}{2\pi} \sum_{E_m < E_F} \int_{\text{BZ}} d^2k (\langle \partial_x u_{m\mathbf{k}} | \partial_y u_{m\mathbf{k}} \rangle - \langle \partial_y u_{m\mathbf{k}} | \partial_x u_{m\mathbf{k}} \rangle) \\ &= \frac{1}{2\pi} \int_{\text{BZ}} \text{Tr}(\mathcal{F}), \end{aligned} \quad (2.8)$$

where the suffix m is the index of the bands from the lowest energy band, the summation is taken over the bands below the Fermi energy E_F , and

$$\mathcal{F} = da - ia \wedge a, \quad (2.9)$$

¹ We assume that the Berry curvature does not depend on time t , because the Hall current is the lowest order in the time-dependent term, when we assume that the time dependence of the system is weak.

with the matrix of the Berry connection $a_{mn} = i \langle u_{m\mathbf{k}} | du_{n\mathbf{k}} \rangle$.² The Chern number ν defined here is shown to be integer. Thus the quantization of the Hall conductivity follows for any band insulators without interaction and disorder.

2.1.1 Integer Quantum Hall Effect as a Topological Insulator

We have seen that the Hall current is described by the Berry curvature, and the Hall conductivity is quantized in the gapped system as $\nu \frac{e^2}{h}$, where ν is an integer. Therefore, to observe the quantized Hall conductivity, ν must be nonzero. Here we discuss the origin of the Hall conductivity, in the case of an insulator with only one occupied band according to Kohmoto [7]. The Hall conductivity is written in terms of the connection as

$$\begin{aligned} \sigma_{xy} &= \frac{e^2}{h} \int_{\text{BZ}} d\mathbf{k} [\nabla_{\mathbf{k}} \times \mathbf{a}]_z \\ &= \frac{e^2}{h} \oint_{\text{BZ}} d\mathbf{k} \cdot \mathbf{a}, \end{aligned} \quad (2.11)$$

where $\mathbf{a} = i \langle u_{n\mathbf{k}} | \nabla_{\mathbf{k}} u_{n\mathbf{k}} \rangle$, we omitted the band index for simplicity, and used the Stokes theorem. We assume that only the n -th band is occupied. The above expression means that the Hall conductivity is invariant under the gauge transformation,

$$|u_{\mathbf{k}}\rangle \rightarrow e^{if_{\mathbf{k}}} |u_{\mathbf{k}}\rangle, \quad (2.12)$$

where $f_{\mathbf{k}}$ is real. On the other hand, the connection depends on the phase; the gauge transformation gives

$$\mathbf{a} \rightarrow \mathbf{a} + \nabla_{\mathbf{k}} f_{\mathbf{k}}. \quad (2.13)$$

In 2Ds, the BZ can be regarded as a torus, and the wavefunction is expected to be periodic. Naively, one might think that the above equation Eq. (2.11) vanishes due to the periodicity because the path of the integral contains the same states with opposite directions (see Fig. 2.1). However, ν becomes nonzero, when the phase of the wavefunction cannot be determined uniquely and smoothly in the whole BZ; in other words, the phase singularity in the BZ cannot be removed by any gauge transformation when ν is not trivial.

To investigate the relation between the phase and the Hall conductivity, we consider an arbitrary eigenstate $|u_{\mathbf{k}}\rangle$ on 2D systems, and we try to determine the phase of

² For a vector $\mathbf{x} = x_1 \mathbf{e}_1 + x_2 \mathbf{e}_2 + x_3 \mathbf{e}_3$ where $\mathbf{e}_{i=1,2,3}$ are the basis vectors, the wedge product \wedge is defined as

$$dx_1 \wedge dx_2 = \mathbf{e}_1 \times \mathbf{e}_2 dx_1 dx_2 = \mathbf{e}_3 dx_1 dx_2. \quad (2.10)$$

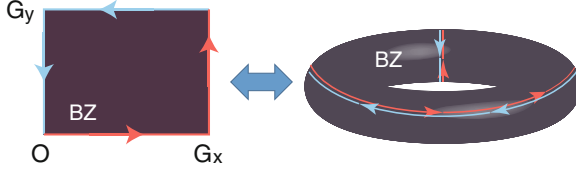


Fig. 2.1 Schematic the 2D BZ. $G_{x,y}$ denote the reciprocal wavevectors for the x and y directions. The *arrows* show the direction of the path integral for the Hall conductivity. In the calculation, the paths with opposite *arrows* cancel with each other, when the phase of the wavefunction is defined smoothly in the whole BZ

the wavefunction in the whole BZ. There is a simple way to determine the phase; we first fix a certain position $\mathbf{r} = (x, y)$, and we require a component of the state vector $|u_{\mathbf{k}}\rangle$ at the position \mathbf{r} , $u_{\mathbf{k}}(\mathbf{r}) = \langle \mathbf{r} | u_{\mathbf{k}} \rangle$, to be real. If $u_{\mathbf{k}}(\mathbf{r})$ has a non vanishing phase $g_{\mathbf{k}}$ which is assumed to be real and smooth, we perform the gauge transformation,

$$|u'_{\mathbf{k}}\rangle = e^{-ig_{\mathbf{k}}} |u_{\mathbf{k}}\rangle, \quad (2.14)$$

where $e^{ig_{\mathbf{k}}} = \frac{u_{\mathbf{k}}(\mathbf{r})}{|u_{\mathbf{k}}(\mathbf{r})|}$, and thus, we can make $u'_{\mathbf{k}}(\mathbf{r})$ to be real.

On the other hand, we cannot do this when the wavefunction vanishes for some \mathbf{k} . For simplicity, we assume that $u_{\mathbf{k}}(\mathbf{r})$ vanishes only at $\mathbf{k} = \mathbf{k}_0$. Then, the phase of $u_{\mathbf{k}}(\mathbf{r})$ cannot be determined at $\mathbf{k} = \mathbf{k}_0$; by the singularity, the phase of the wavefunction $u_{\mathbf{k}}(\mathbf{r})$ is determined except for $\mathbf{k} = \mathbf{k}_0$. Here, we again fix the phase of $u_{\mathbf{k}}(\mathbf{r})$ to be real as Eq. (2.14), for $\mathbf{k} \in \text{BZ} - \{\mathbf{k}_0\}$. To make clear the argument, we divide the BZ into two, H_I and H_{II} ; H_I contains a vicinity of $\mathbf{k} = \mathbf{k}_0$, and H_{II} is the complement of H_I in the BZ. Then, we choose another position \mathbf{r}' such that the component of $u_{\mathbf{k}}(\mathbf{r}')$ does not vanish in the region H_I including $\mathbf{k} = \mathbf{k}_0$. Since $u_{\mathbf{k}}(\mathbf{r}')$ does not have a singularity in H_I , we can impose it to be real by using a real function $h_{\mathbf{k}}$ as

$$|u''_{\mathbf{k}}(\mathbf{r}')\rangle = e^{-ih_{\mathbf{k}}} |u_{\mathbf{k}}(\mathbf{r}')\rangle, \quad (2.15)$$

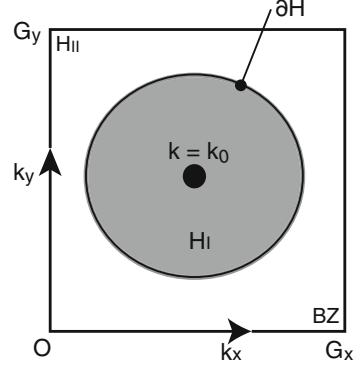
where $e^{ih_{\mathbf{k}}} = \frac{u_{\mathbf{k}}(\mathbf{r}')}{|u_{\mathbf{k}}(\mathbf{r}')|}$. Thus, we have a wavefunction whose phase is defined in the whole BZ in Fig. 2.2.

$$\begin{cases} |u_{\mathbf{k} \in H_I}\rangle = e^{-ih_{\mathbf{k}}} |u_{\mathbf{k}}\rangle \\ |u_{\mathbf{k} \in H_{II}}\rangle = e^{-ig_{\mathbf{k}}} |u_{\mathbf{k}}\rangle \end{cases}. \quad (2.16)$$

The remaining problem is the phase on the boundary between H_I and H_{II} . If the phases can be connected smoothly there, it is inconsistent with the initial assumption that we cannot define the phase to be smooth in the whole BZ. Therefore, there is a phase mismatch at the boundary ∂H ,

$$|u_{\mathbf{k} \in H_I}\rangle = e^{i\eta_{\mathbf{k}}} |u_{\mathbf{k} \in H_{II}}\rangle, \quad (2.17)$$

Fig. 2.2 Schematic of diagram of a phase of a wavefunction. To determine the phase on the entire BZ, it is divided into two regions. At $\mathbf{k} = \mathbf{k}_0$, there is a singularity of the phase for $u_{\mathbf{k}}(\mathbf{r})$



where $t_{\mathbf{k}} = g_{\mathbf{k}} - h_{\mathbf{k}}$. Because the connection depends on the gauge, we define the connections as \mathbf{a}^I and \mathbf{a}^{II} on H_I and H_{II} , respectively. The Hall conductivity coming from the two regions is expressed as

$$\begin{aligned}\sigma_{xy} &= \frac{e^2}{\hbar} \int_{\text{BZ}} d\mathbf{k} [\nabla_{\mathbf{k}} \times \mathbf{a}]_z \\ &= \frac{e^2}{\hbar} \int_{H_I} d\mathbf{k} [\nabla_{\mathbf{k}} \times \mathbf{a}^I]_z + \frac{e^2}{\hbar} \int_{H_{II}} d\mathbf{k} [\nabla_{\mathbf{k}} \times \mathbf{a}^{II}]_z \\ &= \frac{e^2}{\hbar} \nu\end{aligned}\quad (2.18)$$

$$\nu = \frac{1}{2\pi} \int_{\partial H} d\mathbf{k} \cdot (\mathbf{a}^I - \mathbf{a}^{II}) = \frac{1}{2\pi} \int_{\partial H} d\mathbf{k} \cdot \nabla t_{\mathbf{k}}. \quad (2.19)$$

The constant ν defined in Eq. (2.19) is called the Chern number and must be integer because $t_{\mathbf{k}}$ comes from the gauge transformation, and its change around ∂H is an integer multiple of 2π . ν is a topological invariant; it does not change by any smooth deformation of the path ∂H . In addition, since the nontrivial winding of the phase difference $t_{\mathbf{k}}$ is supported by the existence of the singularity, it never changes from the integer by small external perturbation which does not close the band gap.

2.1.2 Adiabatic Charge Polarization by the Berry Phase

In the previous section, we have discussed the Hall current originating from the Berry phase. The Hall current emerges when the quantum states change with time; there is a correspondence between the perturbation and time evolution of the wavenumber. Here, we consider the charge polarization in the form of the Berry phase by an adiabatic change of external perturbations. The Schrödinger equation is given as

$$H(\mathbf{k}, \lambda)|\psi_{\mathbf{k},\lambda}\rangle = E(\mathbf{k}, \lambda)|\psi_{\mathbf{k},\lambda}\rangle, \quad (2.20)$$

where the eigenfunction $|\psi_{\mathbf{k},\lambda}\rangle$ has the Bloch form with $|\psi_{\mathbf{k},\lambda}\rangle = e^{i\mathbf{k}\cdot\mathbf{r}}|u_{\mathbf{k},\lambda}\rangle$, and the wavefunction and the Hamiltonian explicitly depend on a parameter λ representing an external perturbation. λ changes from the initial state with $\lambda = \lambda_i$ to the final state with $\lambda = \lambda_f$ continuously. For example, when we apply pressure the system, the lattice structure is distorted weakly, and this affects the quantum states by the perturbation. Since the Bloch wavefunction spreads out over the system periodically, we use Wannier functions defined as

$$|\mathbf{R}, \lambda\rangle = \frac{1}{\sqrt{N_0}} \sum_{\mathbf{k}} e^{i\mathbf{k}\cdot(\mathbf{r}-\mathbf{R})} |u_{\mathbf{k},\lambda}\rangle, \quad (2.21)$$

where \mathbf{R} specifies one of the lattice sites, and N_0 is the number of lattice sites. Then the polarization \mathbf{P} in units of the electronic charge e is given as

$$\begin{aligned} \mathbf{P}_\lambda &= \langle \mathbf{R}, \lambda | \mathbf{r} | \mathbf{R}, \lambda \rangle \\ &= \sum_{\mathbf{k}} \mathbf{a}_{\mathbf{k},\lambda}, \end{aligned} \quad (2.22)$$

where $\mathbf{a}_{\mathbf{k},\lambda}$ is the previously defined connection, and we used the relation

$$\begin{aligned} (\mathbf{r} - \mathbf{R})|\mathbf{R}, \lambda\rangle &= \frac{1}{\sqrt{N_0}} \sum_{\mathbf{k}} -i(\nabla_{\mathbf{k}} e^{i\mathbf{k}\cdot(\mathbf{r}-\mathbf{R})}) |u_{\mathbf{k},\lambda}\rangle, \\ &= \frac{1}{\sqrt{N_0}} \sum_{\mathbf{k}} \left[-i\nabla_{\mathbf{k}} (e^{i\mathbf{k}\cdot(\mathbf{r}-\mathbf{R})} |u_{\mathbf{k},\lambda}\rangle) + i e^{i\mathbf{k}\cdot(\mathbf{r}-\mathbf{R})} |\nabla_{\mathbf{k}} u_{\mathbf{k},\lambda}\rangle \right]. \end{aligned} \quad (2.23)$$

Therefore the polarization vector after the adiabatic change is given as

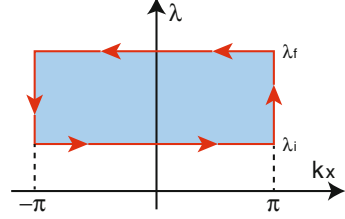
$$\Delta \mathbf{P} = \mathbf{P}_{\lambda_f} - \mathbf{P}_{\lambda_i} = \sum_{\mathbf{k}} (\mathbf{a}_{\mathbf{k},\lambda_f} - \mathbf{a}_{\mathbf{k},\lambda_i}), \quad (2.24)$$

Here, we assume that the wavefunctions for wavevectors different by a reciprocal lattice vector are equal, including the phase. Then the x -component of the polarization is given as

$$\begin{aligned} \Delta P^x &= -\frac{1}{2\pi} \int dk_x (\tilde{a}_{k_x, \lambda_i}^x - \tilde{a}_{k_x, \lambda_f}^x) - \frac{1}{2\pi} \int d\lambda (\tilde{a}_{n\pi, \lambda}^\lambda - \tilde{a}_{n-\pi, \lambda}^\lambda) \\ &= -\frac{1}{2\pi} \oint d(k_x, \lambda) \cdot (\tilde{a}_{k_x, \lambda}^x, \tilde{a}_{k_x, \lambda}^\lambda), \end{aligned} \quad (2.25)$$

where $\tilde{a}_{k_x, \lambda_i}^{x, (\lambda)} = \sum_{k_y, k_z} a_{\mathbf{k}, \lambda_i}^{x, (\lambda)}$, $a_{\mathbf{k}, \lambda_i}^\lambda = \langle u_{\mathbf{k}\lambda} | i \partial_\lambda u_{\mathbf{k}\lambda} \rangle$, and the added term is zero by our assumption. Therefore the charge polarization is described by the contour integral of

Fig. 2.3 Schematic of the path for the integral of the Berry connection



the Berry connection (Fig. 2.3). In addition, by the Stokes theorem, the polarization is represented by the Berry curvature as

$$\Delta P^x = -\frac{1}{2\pi} \oint dk_x d\lambda \tilde{b}_{k_x, \lambda_i}^{x\lambda}, \quad (2.26)$$

$$\tilde{b}_{k_x, \lambda_i}^{x\lambda} = \partial_x \tilde{a}_{k_x, \lambda_i}^\lambda - \partial_\lambda \tilde{a}_{k_x, \lambda_i}^x. \quad (2.27)$$

This polarization can be interpreted as the displacement of the center of the Wannier function, and the piezoelectric effect is studied based on this notion in detail [8, 9]. In particular, when the external perturbation is periodic, ΔP^x becomes an integer.

2.1.3 Laughlin's Gedanken Experiment

Laughlin gave an explanation of the quantization of the Hall conductivity [3], in terms of the gauge invariance. We consider a 2DEG on the xy plane subjected to a strong magnetic field along the z axis. The Hamiltonian is

$$H = \frac{1}{2m} (\mathbf{p} + e\mathbf{A})^2. \quad (2.28)$$

By using the Landau gauge,

$$\begin{cases} A_x = -By \\ A_y = 0 \end{cases}. \quad (2.29)$$

The system has translational symmetry along the x direction, and we impose the periodic boundary condition for the x axis, and the open boundary condition for the y axis with the size $L_x \times L_y$. Hence this system is regarded as a cylinder along the y axis. The Hamiltonian for the 2DEG is expressed as

$$\begin{aligned} H_{k_q} &= e^{-ik_q x} H e^{ik_q x} \\ &= \frac{1}{2m} p_y^2 + \frac{1}{2} m \omega_c^2 (y - k_q \ell^2)^2, \end{aligned} \quad (2.30)$$

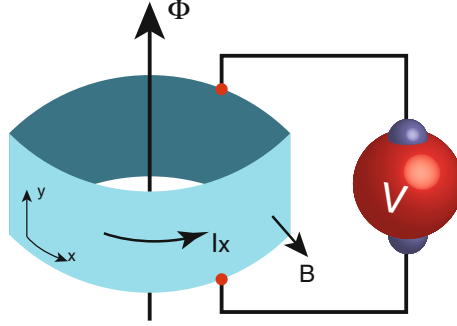


Fig. 2.4 Schematic of the geometry of the 2DEG system. The magnetic field is applied perpendicular to the cylinder. The system is periodic along the x axis, and the flux penetrates the cylinder. Along the y axis, the open boundary condition is imposed and the electronic field is applied. The Hall current is generated by the flux

where $\omega_c = \frac{eB}{m}$ is the cyclotron frequency, $\ell = \sqrt{\frac{\hbar}{eB}}$ is the magnetic length, and the wavenumber is given as $k_q = \frac{2\pi}{L_x}q$ with an integer q . From this Hamiltonian, the eigenstates has the same form as the harmonic oscillator, which has its center at $y_q = k_q \ell^2$. The eigenvalue forms the Landau level, given as

$$\varepsilon_n = \hbar\omega_c \left(\frac{1}{2} + n \right), \quad (2.31)$$

$$n = 0, 1, 2, \dots, \quad (2.32)$$

which does not depend on the wavenumber. When the wavenumber is changed as $q \rightarrow q + 1$, while the energy spectrum is invariant, the center of the eigenstate shifts by $\delta y = \frac{2\pi\hbar}{eBL_x}$. Therefore, the system is invariant under the gauge transformation $\mathbf{A} \rightarrow \mathbf{A} + \delta\mathbf{A}$, where $\delta\mathbf{A} = (\frac{\delta\Phi}{L_x}, 0)$, and $\delta\Phi = \frac{2\pi\hbar}{e}$.

Now, we consider the Fermi energy is on the gap between the Landau levels ε_v and ε_{v+1} . Due to the periodicity along the x axis, the Aharanov-Bohm flux along the cylinder axis is introduced (Fig. 2.4). The change of the energy by the flux is given as

$$\begin{aligned} \delta\langle H \rangle &= \langle H(\mathbf{A} + \delta\mathbf{A}) \rangle - \langle H(\mathbf{A}) \rangle = -\frac{\delta\Phi}{L_x} \int_0^{L_x} \int_0^{L_y} d\mathbf{r} j_x \\ &= -\delta\Phi I_x \end{aligned} \quad (2.33)$$

where $\langle \mathcal{O} \rangle$ denotes the average value of the operator \mathcal{O} , I_x is the current along the x axis, the current density is given as

$$j_x = -e \left\langle \frac{p_x + eA_x}{m} \right\rangle = - \left\langle \frac{\partial H}{\partial A_x} \right\rangle, \quad (2.34)$$

and we used the invariance of the states under the flux change $\delta\mathbf{A}$. Therefore, the Hall current is given as the change of energy by the fictitious flux as

$$I_x = -\frac{\delta\langle H \rangle}{\delta\Phi}. \quad (2.35)$$

The change of the energy is estimated by the movement of the electron gas. Since the voltage $V(y)$ is applied along the y axis, the electrons are subjected to the electronic field $\frac{V(L_y)-V(0)}{L_y}$, and all of the electrons move along the y axis by $\delta y = \frac{2\pi\ell^2}{L_x}$ by the flux. Therefore $\delta\langle H \rangle$ is given as

$$\begin{aligned} \delta\langle H \rangle &= -e\delta y \times \frac{V(L_y) - V(0)}{L_y} \times vN_0 \\ &= -ev(V(L_y) - V(0)) \end{aligned} \quad (2.36)$$

where $N_0 = \frac{L_x L_y}{2\pi\ell^2}$ is the degeneracy of one Landau level.³ Therefore, we have the current as

$$I_x = v \frac{e^2}{h} (V(L_y) - V(0)), \quad (2.37)$$

with the quantized conductivity $v \frac{e^2}{h}$. The calculation of the change of the energy corresponds to the integral of the current density j_x with respect to the wavenumber k_x , since the momentum has the covariant form, $\mathbf{k} + e\mathbf{A}$. In another perspective, charges move along the y axis by δy by the flux insertion, and therefore the charge polarization occurs.

In this context, we discuss the charge polarization previously mentioned in Sect. 2.1.2. We consider the 2DEG system with the periodic boundary condition along the x and y axes. The system can be regarded as a torus, and the flux penetrates along the y axis. By the flux $\delta\Phi$, the variation of the gauge is given as $\delta\mathbf{A} = (0, \frac{\delta\Phi}{L_y})$, and a change of the charge polarization at k_y along the x axis becomes

$$\Delta P^x(k_y) = \frac{1}{2\pi} \int dk_x (a_{x\mathbf{k}+e\delta\mathbf{A}} - a_{x\mathbf{k}}). \quad (2.38)$$

Since the flux causes the momentum shift, the total polarization is given as

$$\begin{aligned} \Delta P^x &= \sum_{k_y=0}^{G_y} \Delta P^x(k_y) = \frac{1}{2\pi} \int dk_x (a_{x\mathbf{k}+(0,G_y)} - a_{x\mathbf{k}}) \\ &= -\frac{1}{2\pi} \int d\mathbf{k} b_z(\mathbf{k}). \end{aligned} \quad (2.39)$$

³ When the Landau level is filled, the electron density per Landau level is given as $\frac{N_0}{L_x L_y} = \frac{eB}{h} = \frac{1}{2\pi\ell^2}$.

Therefore, the change of the charge polarization by flux insertion is also described by the Chern number.

We have seen the states move in momentum space by the flux insertion. This movement and the electronic current imply existence of the electronic states crossing the Fermi energy, which cannot be seen in the bulk states. Indeed, these hidden states are localized at edge, and this fact is consistent with the quantized conductivity that does not depend on the size of the system. Thus, we conclude that the Chern number is an indication of the boundary states carrying the quantized conductivity. While the Chern number is defined as a quantity in the bulk with translational symmetry, remarkably, we can extract information of the boundary states from it. This is a basic notion of the bulk-boundary correspondence, which has been applied to broad classes of topological insulators.

2.1.4 Physical Picture of the Edge State

The topological order in the QH effect manifests itself in the existence of the edge states, which is localized on the edge of system, and the quantized conductivity is carried by the edge channel. In this section we explain an intuitive picture of edge states proposed by Halperin and Büttiker [10, 11]. We assume a 2DEG system in the xy plane with a magnetic field \mathbf{B} along the z axis, and an electric field \mathbf{E} is applied along the y axis (Fig. 2.5a). The classical velocity of the center of the cyclotron motion \mathbf{v}_c is given as

$$\mathbf{v}_c = \frac{\mathbf{E} \times \mathbf{B}}{B^2}. \quad (2.40)$$

For the n -th Landau levels, the energy of the edge states E_n is described as

$$E_n = -eW(\mathbf{r}) + \hbar\omega_c \left(\frac{1}{2} + n \right), \quad (2.41)$$

where ω_c is the cyclotron frequency, and $-eW(\mathbf{r})$ is the confinement potential at the position \mathbf{r} (Fig. 2.5b). The density of states in each Landau level per unit area is $\frac{Be}{h}$. Therefore, the Hall current density j_x^n for the n -th Landau level is given as

$$j_x^n = -e \left(\frac{Be}{h} \right) \theta \left(\mu - eW(\mathbf{r}) + \hbar\omega_c \left(\frac{1}{2} + n \right) \right) \left(-\frac{1}{B} \frac{\partial W}{\partial y} \right), \quad (2.42)$$

where we use $v_{cx} = \frac{E_y}{B} = -\frac{1}{B} \frac{\partial W}{\partial y}$ due to the confinement, and μ is the chemical potential. The Hall current I_x^n at the edge is given as

$$I_x^n = \frac{e^2}{h} \int_0^{L_y} dy \theta \left(\mu - eW(\mathbf{r}) + \hbar\omega_c \left(\frac{1}{2} + n \right) \right) \left(\frac{\partial W}{\partial y} \right). \quad (2.43)$$

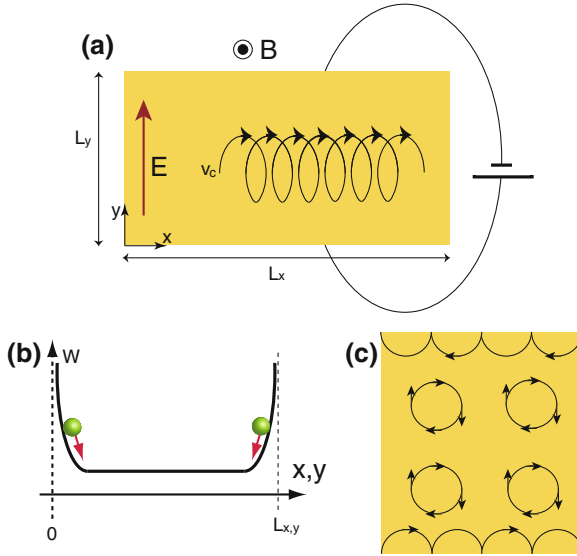


Fig. 2.5 **a** Schematic of a 2DEG system. The magnetic field B is applied along the z axis, and the electric field E is along the y axis. The *curve* illustrates a cyclotron motion with the classical velocity v_c . **b** Schematic of the confinement potential W . W is divergent outside of the system. The *balls* represent electrons confined within the system, and the *arrows* show the directions of the force due to the effective electric field $\frac{\partial W}{\partial \mathbf{r}}$. **c** Schematic of the cyclotron motion in a 2DEG system. The cyclotron motion is illustrated as *circles* whose *arrows* represent the direction of the motion. The neighboring motions cancel each other, and only the skipping orbits at the edge remain

When $\mu > E_n(\mathbf{r})$ for any $\mathbf{r} \in [0, L_x] \times [0, L_y]$, the Hall current is given as

$$I_x^n = \frac{e^2}{h} (W(L_y, x) - W(0, x)) = \frac{e^2}{h} V, \quad (2.44)$$

where we use the fact that the difference of the confinement potential corresponds to the electric voltage V in the y direction. When the n -th Landau level with $0 \leq n \leq \nu - 1$ is filled, the Hall current I_x is given by

$$I_x = \nu \frac{e^2}{h} (W(L_y, x) - W(0, x)) = \nu \frac{e^2}{h} V, \quad (2.45)$$

which is a well-known result for the integer QH effect. In this case, each Landau level is shown to have the Chern number unity. Then we can see that Eq. (2.45) is a special case of Eq. (2.7).

We note that the edge mode is interpreted also from the picture of a collection of the cyclotron motions. In the collection of the cyclotron motions under the magnetic field, they cancel each other in the bulk, but do not on the edge. Only the cyclotron motions forming skipping orbits along the edges remain on the edges, and they make

the edge current called the chiral edge states (Fig. 2.5c). From this intuitive picture, we see that the direction of the chiral edge mode results from that of the cyclotron motion.

2.1.5 Berry Curvature in Systems with Broken Time-Reversal Symmetry

So far, the QH effect is shown in the 2DEG in a magnetic fields. Each Landau level is labeled with the Chern number $n_c = 1$, and Chern numbers of the system corresponds to the number of the occupied Landau levels. In this case, the magnetic field is important to generate the QH effect. In a time-reversal invariant system the Hamiltonian H satisfies the relation

$$\Theta H(\mathbf{k}) \Theta^{-1} = H(-\mathbf{k}), \quad (2.46)$$

where \mathbf{k} is the wavevector, and the time-reversal operator $\Theta = i\sigma_y K$ is represented by the product of the y -component of the Pauli matrix σ_y acting on spin degrees of freedom and the complex conjugation operator K . If the system has the time-reversal symmetry, the Chern number ν vanishes because the Berry curvature satisfies the relation (Sect. 6.1.1),

$$\mathbf{b}(\mathbf{k}) = -\mathbf{b}(-\mathbf{k}). \quad (2.47)$$

Conversely, a nonzero Chern number requires breaking of time-reversal symmetry. In the normal QH effect, magnetic fields are used to break time-reversal symmetry. However magnetic fields are not necessary to realize the QH effect, as in the case for the Haldane model [12]. On the other hand, in time-reversal-invariant systems, we need another scheme for topological characterization in terms of a new topological invariant. It leads to the Z_2 topological number, as is introduced in the next section.

2.2 Topological Insulator

Topological insulators are new states of matter, which are proposed by Kane and Mele, and by Bernevig and Zhang [13–18]. In TIs, the bulk is gapped while the boundary of the system is metallic and they are realized in the presence of time-reversal symmetry. Strong spin-orbit interaction (SOI) is required to realize TIs.

The two-dimensional (2D) TI was first proposed in graphene, and the gap is formed by the spin-orbit interaction. However, the SOI is too small to realize the 2DTI in graphene in experiments. After that proposal, Bernevig et al. theoretically predicted realization of the 2DTI in HgTe quantum well in 2006 [15], and in 2007 König

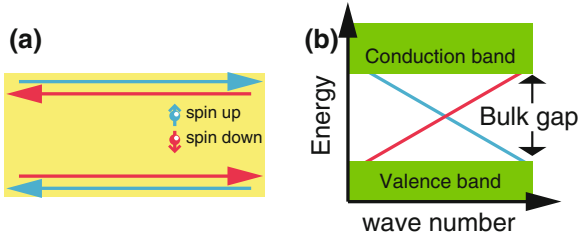


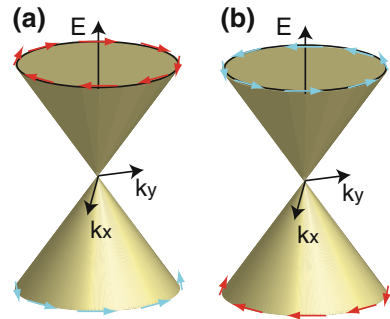
Fig. 2.6 Schematics illustrating edge states of 2DTIs. **a** The edge current of the 2DTI in the ribbon geometry, **b** The dispersion of the edge states is shown as *blue* and *red* lines. There are two states with opposite directions of velocities and opposite spins, forming a Kramers pair

et al. observed the 2DTI through the quantized edge conductivity in the quantum well [19]. In 2DTIs, there are edge states consisting of a pair of spin-filtered states, whose spins and velocities are opposite to each other due to the Kramers's theorem (Fig. 2.6a). Such edge states consisting of counterpropagating states are called helical edge states. The 2DTI can be understood as a superposition of two QH systems with opposite magnetic fields for the two spin states (Fig. 2.6b).

In 2007 three-dimensional (3D) TIs were predicted theoretically [16, 17, 20] and $\text{Bi}_{1-x}\text{Sb}_x$ was predicted as a 3DTI [17]. Subsequently they were realized in experiments: $\text{Bi}_{1-x}\text{Sb}_x$ [21], Bi_2Se_3 [22, 23] and Bi_2Te_3 [24]. Since then, the search for 3DTI has been ongoing actively. An effective theory for the surface states of the 3DTI is described by the massless Dirac equation. The dispersion is linear in the wavevector, and typically the spin is perpendicular to the wavevector. There are two possibilities for the relation between the spin and wavevector (Fig. 2.7), called chirality. Materials which were identified as 3DTIs such as Bi_2Se_3 , and Bi_2Te_3 have the chirality illustrated in Fig. 2.7a. A recent experiment shows that the surface states in $\text{Bi}_4\text{Se}_{2.6}\text{S}_{0.4}$ have the opposite chirality from these materials (Fig. 2.7b) [25].

Transport phenomena by these boundary states in TI are unique. In the edge states of 2DTIs, the back-scattering is prohibited, and therefore the edge channel perfectly conducts. This is because the two states within the edge channels form a

Fig. 2.7 Schematics of the dispersion of the surface states (**a**, **b**). The *circle* shows the Fermi surface of the surface states above the Dirac point, and the *arrows* pointing along the Fermi surface are spins. **a** and **b** correspond to opposite chiralities



Kramers pair, and backscattering between them is prohibited; the gapless edge states are robust against impurities as long as time-reversal symmetry is preserved [26, 27]. On the other hand, in 3DTIs the surface current is diffusive because impurity scatterings occur unlike the edge states in 2DTIs. As an application of the transport in TIs, thermoelectric phenomena have been studied. For the thermoelectronic figure of merit [28, 29], it is generally known that low-dimensionality is favorable [32, 33]. There are metallic states which are localized at the edges of TIs, and in several papers, enhanced thermoelectric transport has been reported by using the edge states of TIs [30, 31, 34].

2.2.1 Topological Invariant Under Time-Reversal Symmetry

Systems under time-reversal symmetry are characterized by the Z_2 topological numbers. The Z_2 topological number was first introduced in 2D systems [13–16, 35]. Then later, the theory was extended to 3D [17]. In the following, we explain the idea of the Z_2 topological number.

By the time-reversal symmetry, the Bloch wavefunctions $|u(\mathbf{k})\rangle$ and $|\Theta u(\mathbf{k})\rangle$ are degenerate, and orthogonal to each other (Sect. 6.2). This is the Kramers theorem; the dispersion is symmetric with respect to \mathbf{k} because the wavevector of the states $|\Theta u(\mathbf{k})\rangle$ is $-\mathbf{k}$, and therefore the states at \mathbf{k} and $-\mathbf{k}$ have opposite spins from each other. The energy spectra necessarily cross and the states are doubly degenerate by Kramers's theorem at time-reversal invariant momenta (TRIM) $\mathbf{k} = \mathbf{\Gamma}$ where $\mathbf{\Gamma} = -\mathbf{\Gamma} \pmod{\mathbf{G}}$ and \mathbf{G} is a reciprocal lattice vector; in other words, the degeneracy at the TRIM is protected as long as time-reversal symmetry is preserved.

In systems with time-reversal symmetry, the Chern number vanishes because Berry curvatures contributed from $|u\rangle$ and $|\Theta u\rangle$ cancel each other. We first consider a special situation where the states are eigenstates of the spin along z , $s_z = \pm$ and the two subspaces with $s_z = +$ and $s_z = -$ are decoupled. Therefore $|u\rangle$ and $|\Theta u\rangle$ have opposite spins to each other, and are labeled with $s_z = \pm$. Then edge currents from $s_z = \pm$ states run along opposite directions with opposite spins due to the SOI as the driving force [36–41], which does not break time-reversal symmetry. Therefore in this simple case we can construct a topological invariant (Chern number) for each subspace with $s_z = \pm$. Namely the two subspaces from $s_z = \pm$ have Chern numbers with opposite signs to each other. When these Chern numbers are not zero, as we learned in Sect. 2.1.4, we have the charge polarizations when the wavefunction is changed adiabatically by a reciprocal lattice vectors, and it leads to the topological edge states.

This notion is generalized in terms of time-reversal polarization [35] when s_z is no longer conserved; in a general system with time-reversal symmetry, the two subspaces $s_z = +$ and $s_z = -$ are not decoupled, and the Chern numbers within each sector cannot be defined. Hence, in general cases, topological invariants are directly given by the difference of the charge polarizations between the pairs connected by time-reversal operation: $|u\rangle$ and $|\Theta u\rangle$. For 2D systems, by calculating the difference of the charge polarizations by using Eq. (2.39), under a change of wavevector by a

half of the reciprocal lattice vector along the x axis, the Z_2 topological number ν is defined as

$$\nu \equiv \frac{1}{2\pi} \left[\int_{\mathbf{BZ}_{1/2}} \text{Tr}(\mathcal{F}) - \oint_{\partial \mathbf{BZ}_{1/2}} \text{Tr}(a) \right] \pmod{2} \quad (2.48)$$

where $\mathbf{BZ}_{1/2}$ means a half of the BZ. The topological number takes $\nu = 1$ for topologically nontrivial systems or $\nu = 0$ for ordinary insulators. This expression coincides with the above discussion because the integration of $\text{Tr}(\mathcal{F})$ over half of the BZ means the polarization contributed from one of the Kramers pair. We note that the definition of the Z_2 topological number Eq. (2.48) can be extended to 3DTIs.

The Z_2 topological number can be represented by a more convenient form. To this end, we define the following $2N \times 2N$ matrix as

$$w_{mn}(\mathbf{k}) = \langle u_{-\mathbf{k},m} | \Theta | u_{\mathbf{k},n} \rangle, \quad (2.49)$$

where m, n are band indices, which run over occupied bands, and $2N$ is the total number of occupied bands. At each TRIM $\Gamma_{i=1,2,\dots,M}$, an index $\delta_i = \pm 1$ is defined as

$$\delta_i \equiv \frac{\sqrt{\det[w(\Gamma_i)]}}{\text{Pf}[w(\Gamma_i)]}, \quad (2.50)$$

and then the Z_2 topological number ν is defined as

$$(-1)^\nu \equiv \prod_{i \in \text{TRIM}}^M \delta_i, \quad (2.51)$$

where M is the number of TRIM in the BZ e.g., $M = 4$ in 2D, $M = 8$ in 3D.⁴ Due to $\text{Pf}[w(\Gamma_i)]^2 = \det[w(\Gamma_i)]$ there seems to be an ambiguity in the sign of $\sqrt{\det[w(\Gamma_i)]}$ relative to $\text{Pf}[w(\Gamma_i)]$. It is uniquely determined by defining the wavefunction smoothly between TRIM in the BZ. For this purpose we define the function as

$$e^{i\theta(\mathbf{k})} \equiv \frac{\det[w(\mathbf{k})]}{|\det[w(\mathbf{k})]|}. \quad (2.52)$$

We consider a path between two TRIM $\Gamma_{a,b}$ in the BZ, and vary the phase $e^{i\theta(\mathbf{k})}$ smoothly along the path. At Γ_a and Γ_b , we define $\theta_0(\Gamma_a)$ and $\theta_0(\Gamma_b)$ as

$$e^{i\frac{\theta_0(\Gamma_i)}{2}} \equiv \frac{\text{Pf}[w(\Gamma_i)]}{|\text{Pf}[w(\Gamma_i)]|}. \quad (2.53)$$

⁴ In 1D the Z_2 topological number cannot be defined. For example, by a gauge transformation $|u\rangle \rightarrow e^{ik/(2\Gamma)}|u\rangle$ where Γ is a half of the reciprocal lattice vector, the Z_2 topological number changes as $(-1)^\nu \rightarrow -(-1)^\nu$.

Then, by going from Γ_a to Γ_b , the gained phase of the determinant of $w(\mathbf{k})$ is

$$\theta_0(\Gamma_b) - \theta_0(\Gamma_a) + 2\pi \Delta_{ab}, \quad (2.54)$$

where Δ_{ab} is an integer. The adiabatic transition of the phase is expressed as

$$\sqrt{\frac{\det[w(\Gamma_b)]}{|\det[w(\Gamma_b)]|}} \sqrt{\frac{|\det[w(\Gamma_a)]|}{\det[w(\Gamma_a)]}} = e^{i \frac{\theta_0(\Gamma_b) - \theta_0(\Gamma_a)}{2} + \pi i \Delta_{ab}} \quad (2.55)$$

From Δ_{ab} , we define another index related with the time-reversal polarization π_{ab} as

$$\pi_{ab} \equiv \delta_a \delta_b = e^{\pi i \Delta_{ab}}. \quad (2.56)$$

When the phase turns even (odd) times in the Gauss plane $\delta_a \delta_b = +1(-1)$. By using Eq. (2.56), the Z_2 topological number (Eq. 2.51) is calculated. Figure 2.8 shows an example of the calculation of ν in a 2D system with a function $R(\mathbf{k}) = e^{i\theta}$. In this case we have $\delta_1 \delta_2 = -1$ and $\delta_3 \delta_4 = +1$ for the paths $\Gamma_1 \rightarrow \Gamma_2$ and $\Gamma_3 \rightarrow \Gamma_4$, respectively; it leads to $\nu = 1$, and the system is a TI. There are edge states which cross the Fermi energy.

2.2.1.1 Z_2 Topological Number in 3D and Phase Transitions

In 3Ds, there are eight TRIM in the BZ which are described as

$$\Gamma_{\mathbf{n}} = \frac{1}{2}(n_1 \mathbf{G}_1 + n_2 \mathbf{G}_2 + n_3 \mathbf{G}_3), \quad (2.57)$$

where $n_{i=1,2,3} = 0, 1$, The Z_2 topological numbers ($\nu_0; \nu_1, \nu_2, \nu_3$) are defined as

$$(-1)^{\nu_k} \equiv \prod_{n_k=1; n_{j \neq k}} \delta_{\mathbf{n}}. \quad (2.58)$$

where $k = 1, 2, 3$, and ν_0 is described by Eq. (2.51) for $M = 8$. For $\nu_0 = 1$ the system is in the topologically non-trivial phase, called a strong TI, which has an odd number of Dirac cones as the surface states. Strong TIs are also simply called as TI, because the novel surface states are guaranteed by the Kramers theorem. On the other hand for $\nu_0 = 0$, there are an even number of Dirac cones as the surface states, and the system is called a weak TI. In weak TIs, the systems can be regarded as stacked layers of 2DTI. By using the indices (ν_1, ν_2, ν_3) the normal vector of the layers constituting the weak TI is described as

$$\mathbf{G}_\nu = \nu_1 \mathbf{G}_1 + \nu_2 \mathbf{G}_2 + \nu_3 \mathbf{G}_3. \quad (2.59)$$

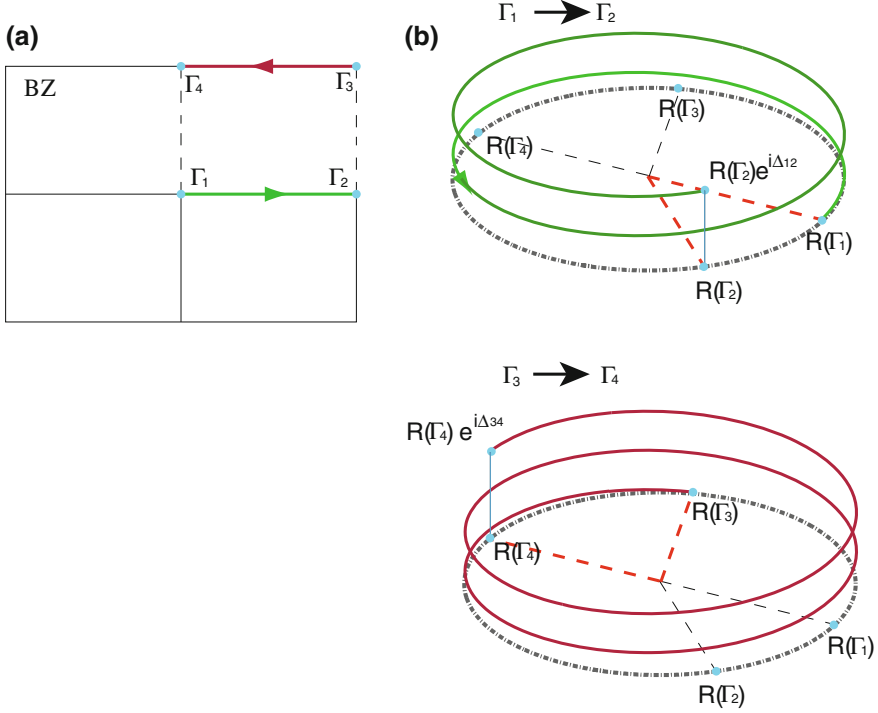


Fig. 2.8 Schematic example of the calculation of ν in a 2D system. $R(\mathbf{k})$ is the phase of Eq. (2.52), plotted as $e^{iR(\mathbf{k})}$ in the complex plane. **a** The BZ of a 2D system and TRIM. **b** The change of the phase (Eq. 2.52) in each path between TRIM. In this case we have $\delta_1\delta_2 = -1$ and $\delta_3\delta_4 = +1$ for the paths $\Gamma_1 \rightarrow \Gamma_2$ and $\Gamma_3 \rightarrow \Gamma_4$, respectively; namely $\nu = 1$, and the system is a strong TI

The weak TI is similar to ordinary insulators, because it includes trivial band insulators, and even if there are nonzero number of Dirac cones as the surface states, the gapless states are fragile against impurities or defects.

To illustrate the surface states of strong and weak TIs, we define an index associated with each surface TRIM as

$$\pi_{n_1, n_2}^z \equiv \delta_{(n_1, n_2, 0)} \delta_{(n_1, n_2, 1)}. \quad (2.60)$$

In the 2D, we have explained that bound states cross the Fermi surface between TRIM with different time-reversal polarizations. Then the Fermi surface on the (001) surface is illustrated as Fig. 2.9 schematically. In Fig. 2.9a the system is the strong TI with $(\pi_{0,0}^z, \pi_{1,0}^z, \pi_{0,1}^z, \pi_{1,1}^z) = (1, 1, 1, -1)$. In this case there is a single-Dirac cone whose Fermi surface encloses $\tilde{\Gamma}_{11}$. On the other hand for $(\pi_{0,0}^z, \pi_{1,0}^z, \pi_{0,1}^z, \pi_{1,1}^z) = (-1, 1, 1, -1)$ (Fig. 2.9b), the system is the weak TI with an even number of Dirac cones.

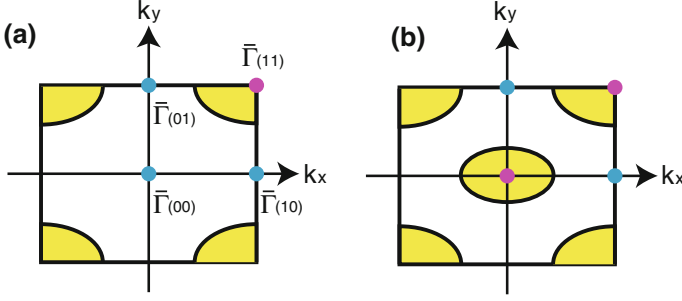


Fig. 2.9 Schematic examples of surface Fermi surfaces for the (001) surface. $\bar{\Gamma}_{n_1 n_2}$ are TRIM of the surface BZ. Curves represent possible Fermi surfaces in the strong TI (a) $(\pi_{0,0}^z, \pi_{1,0}^z, \pi_{0,1}^z, \pi_{1,1}^z) = (1, 1, 1, -1)$, and in the weak TI (b) $(\pi_{0,0}^z, \pi_{1,0}^z, \pi_{0,1}^z, \pi_{1,1}^z) = (-1, 1, 1, -1)$. Blue and red dots represent TRIM with $\pi^z = +1$ and $\pi^z = -1$ respectively

The Z_2 topological number ν is also discussed in the context of the topological field theory without interactions [42, 43]. In the theory, the effective action for electromagnetic fields S_{eff} in TIs is expressed as

$$S_{\text{eff}} = S_{\text{Maxwell}} + S_{\text{topo}} = \int d^3x dt \left[\frac{1}{16\pi} F^{\mu\nu} F_{\mu\nu} + \frac{\alpha\theta}{32\pi} \epsilon^{\mu\nu\sigma\tau} F^{\mu\nu} F_{\sigma\tau} \right], \quad (2.61)$$

where $F^{\mu\nu}$ is the field strength of the electromagnetic fields, S_{Maxwell} describes the conventional electromagnetic action, S_{topo} is characteristic in TIs, $\epsilon^{\mu\nu\sigma\tau}$ is the antisymmetric tensor, α is the fine-structure constant and $\theta = \pi\nu$. From S_{topo} , the Lagrangian $\mathcal{L}_{\text{topo}}$ is described as

$$\mathcal{L}_{\text{topo}} = \theta \frac{e^2}{2\pi h} \mathbf{E} \cdot \mathbf{B}. \quad (2.62)$$

This causes the magnetoelectric effect [42, 44], where the time-reversal symmetry needs to be broken. Due to the correspondence between ν and θ , trivial insulators have $\nu = 0$ and S_{topo} vanishes. In this theory ν is described as

$$\nu = \frac{\theta}{\pi} \equiv \frac{1}{4\pi^2} \int \text{Tr} \left(a \wedge da + i \frac{2}{3} a \wedge a \wedge a \right). \quad (2.63)$$

This is also known as the Chern-Simons term in the quantum field theory.

2.2.1.2 Z_2 Topological Number with Inversion Symmetry

When the system is invariant under the parity transformation (space inversion), the index δ_i is given as [45]

$$\delta_i = \prod_m^N \xi_{2m}(\Gamma_i), \quad (2.64)$$

where $\xi_{2m}(\Gamma_i)$ is the eigenvalue of the parity operator P of the $2m$ -th band at a TRIM Γ_i and it takes the value $\xi_{2m}(\Gamma_i) = \pm 1$. This formula (2.64) was proposed by Fu and Kane. From this formula, $\text{Bi}_{1-x}\text{Sb}_x$ for $0.07 < x < 0.22$ was predicted as a TI. At each TRIM, each band is doubly degenerate due to the Kramers theorem; the $2m$ -th and $2m + 1$ -th bands have the same eigenvalue. This representation makes clear the condition when the topological phase transition occurs. We consider a case where there are $2N$ filled bands and the Fermi energy is in the gap between the $2N$ -th and $2(N + 1)$ -th bands. A 2×2 Hamiltonian H of the $2N$ -th and $2(N + 1)$ -th bands on a TRIM Γ_i are represented as

$$H = \begin{pmatrix} \Delta & 0 \\ 0 & -\Delta \end{pmatrix}, \quad (2.65)$$

where $\pm\Delta$ are the energy eigenvalues of the bands. Due to the degeneracy, we omit the eigenstates of $2N - 1$ -th and $2N + 1$ -th bands from the representation of the Hamiltonian. The eigenstates are

$$|\psi_0\rangle = \begin{pmatrix} 1 \\ 0 \end{pmatrix}, \quad |\psi_1\rangle = \begin{pmatrix} 0 \\ 1 \end{pmatrix}, \quad (2.66)$$

where $|\psi_a\rangle$ represents the eigenstate of the $2(N + a)$ -th band for $a = 0, 1$, with the eigenvalue of the parity as P_a (Fig. 2.10). We treat Δ as a tunable parameter, and the Fermi energy is assumed to be zero.⁵ δ_i becomes

$$\delta_i = \begin{cases} \prod_m^{N-1} \xi_{2m}(\Gamma_i) P_1 & (\Delta > 0), \\ \prod_m^{N-1} \xi_{2m}(\Gamma_i) P_0 & (\Delta < 0). \end{cases} \quad (2.67)$$

When P_0 and P_1 are of opposite signs, the time-reversal polarization changes with the sign of Δ . We further assume that the tuning of Δ does not affect any other states on TRIM. In this case when Δ gets across zero, a phase transition occurs. Namely, when the Fermi energy is sandwiched between bands with opposite eigenvalues of the parity,⁶ either of the following two cases occurs; (i) the phase is a TI or (ii) the phase is a normal insulator and it becomes a TI if the gap is inverted. The Z_2 topological numbers were also calculated by this formula in Bi_2Te_3 and Bi_2Se_3 [46]. The calculation predicted that they are TIs with a single-Dirac cone on the Fermi surface, which well agrees with experiments in these materials [22–24].

⁵ We assume the tuning affect only the four bands around the Fermi energy.

⁶ For example ψ_1 consists of s-orbitals, and ψ_2 consists of p-orbitals.

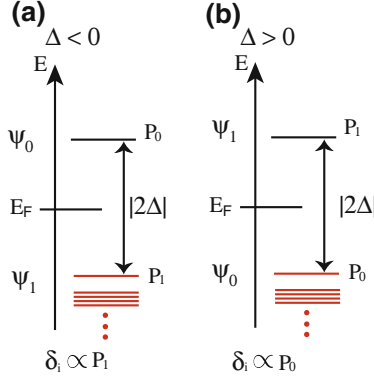


Fig. 2.10 Schematics of energy spectra. E_F is the Fermi energy, δ_i is the index related with the time-reversal polarization, $\psi_{0,1}$ and $P_{0,1}$ are states of the $2N$ -th and $2(N+1)$ -th bands and the parity eigenvalues. $\delta_i \propto P_1$ for **a** $\Delta > 0$, and $\delta_i \propto P_0$ for **b** $\Delta < 0$. When P_0 and P_1 have opposite signs, the index δ_i changes the sign by tuning Δ from $\Delta < 0$ to $\Delta > 0$

2.2.2 Surface Effective Hamiltonian

When a system is in the Z_2 non-trivial phase, the surface states can be obtained from the bulk Hamiltonian by imposing appropriate boundary conditions. This can also be done by using a low-energy effective model [46–48]. Near the TRIM where the surface states are degenerate, called the Dirac point, the surface Hamiltonian H_s and its eigenvalue E_s are expressed as

$$H_s(\mathbf{k}) = v(\sigma_x k_y - \sigma_y k_x), \quad (2.68)$$

$$E_s = s|\mathbf{v}\mathbf{k}| \quad (2.69)$$

where v is the Dirac velocity and the sign of $s(= \pm)$ corresponds to the upper or lower Dirac cones.⁷ The eigenstate ψ_s is given as

$$\psi_s = \frac{1}{\sqrt{2}} \begin{pmatrix} i s \\ \frac{v}{|v|} e^{i\phi_{\mathbf{k}}} \end{pmatrix} e^{i\mathbf{k} \cdot \mathbf{r}}, \quad (2.70)$$

where $\phi_{\mathbf{k}} = \arctan\left(\frac{k_y}{k_x}\right)$ and \mathbf{r} represent the coordinate on the surface. The sign of the velocity $\frac{v}{|v|}$ corresponds to the chirality, (a) or (b) in Fig. 2.7. They are topologically distinguished when the system has mirror symmetry. This correspondence will be discussed in Chap. 3 in detail.

⁷ The Hamiltonian (Eq. 2.68) is transformed into $v(\boldsymbol{\sigma} \cdot \mathbf{k})$ by the unitary transformation, which is known as the massless Dirac Hamiltonian. Therefore we call Eq. (2.68) as the Dirac Hamiltonian.

2.3 Topological Flat-Band States in Honeycomb Lattice

Previously, we have seen emergence of edge states in topological insulators. Here, we review flat-band states on edges. Manifestation of the edge states in this class is supported by metallic bulk states. A similar type of the flat-band states will be discussed in Chap. 4, and the origin of the edge states is explained. Flat bands have been studied particularly in the context of possible ferromagnetism driven by interactions, as was proposed by Lieb [49], and successively by Mielke and Tasaki [50–53]. On the other hand, from the research on graphene [54] it is known that the tight-binding model with nearest-neighbor hopping on a honeycomb lattice with a zigzag edge exhibits flat-band edge states [55], and its origin is topologically interpreted [56]. In addition, the flat-band edge states can be seen in the 3D diamond lattice model [57].

Here we review the flat-band states in the honeycomb lattice model and discuss their topological origin. In the dispersion of a graphene ribbon with zigzag edges, the flat-band edge states appear between the wavenumbers corresponding to the projection of Dirac points at K and K'. In contrast, there are no flat-band edge states in the graphene ribbon with armchair edges, because in the projection of the dispersion, Dirac cones at the K and K' points overlap each other.

When the hopping of the tight-binding model on the honeycomb lattice becomes anisotropic, the Dirac points in the bulk BZ move away from the K and the K' points. Moreover, when the anisotropy is sufficiently large, the two Dirac points meet and the bulk dispersion relation becomes linear in one direction and quadratic in the other [58]. In that case, the flat-band edge states cover the whole one-dimensional (1D) BZ [59]. With a further increase of the anisotropy, the bulk becomes gapped while the completely flat band remains in the edge BZ.

2.3.1 Dispersion of the Honeycomb Lattice Model

We first review the flat-band edge states on the honeycomb-lattice structure shown in Fig. 2.11a, and study the completely flat band for the models with anisotropy, which has been studied by Delplace et al. [59]. We consider a tight-binding Hamiltonian on this lattice,

$$H = \sum_{\langle ij \rangle} c_i^\dagger t_{ij} c_j, \quad (2.71)$$

where t_{ij} is the hopping integral along the nearest-neighbor bond vector τ_a , and c_i (c_i^\dagger) is the annihilation (creation) operator of the electron. We treat the hopping integral t_{ij} as a real positive parameter, and it is labeled with the vectors τ_a as t_a . The bulk Hamiltonian matrix $H_b(\mathbf{k})$ at wavevector \mathbf{k} is given as

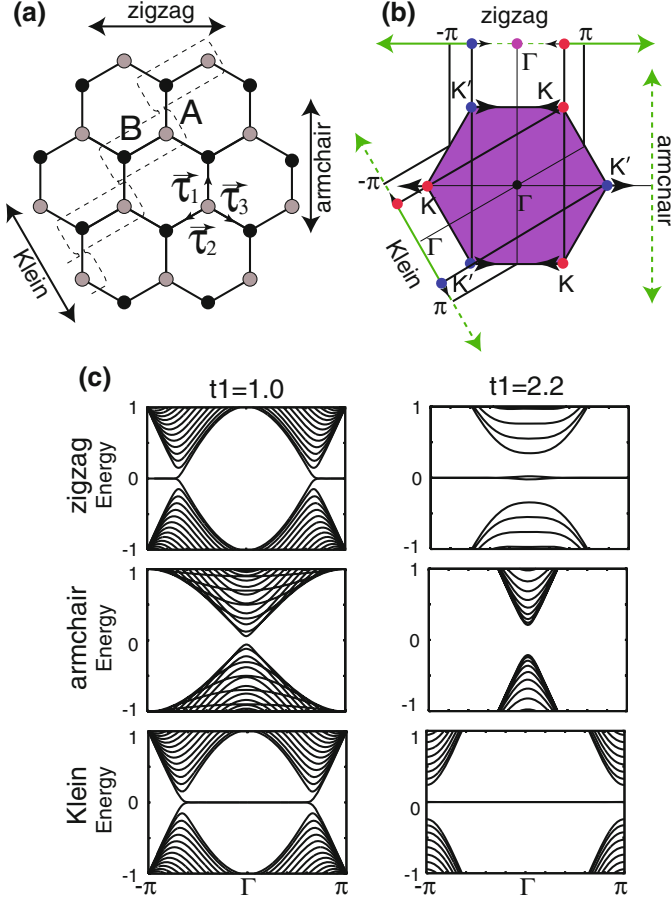


Fig. 2.11 **a** Schematic of the honeycomb-lattice structure. The *dotted line* shows a choice of unit cell with translational symmetry along the edge. The *arrows* show the directions along zigzag, armchair, and Klein edges. **b** The first BZ of the honeycomb lattice. *Dots* at the zone corners show the gap-closing points for the graphene model ($t_1 = t_2 = t_3 = 1$). Namely, the bulk bands become gapless at K and K' points, when the hopping integral is isotropic. By increasing t_1 from unity, the gap-closing points move away from K and K' points as shown by the *arrows*. The flat-band edge states expand in the BZ as the bulk gap-closing points move. **c** The dispersions of ribbons for $t_1 = 1$ and 2.2 at $t_2 = t_3 = 1$, with zigzag, armchair and Klein edges. In zigzag and Klein edges, flat bands appear at the zero energy

$$H_b(\mathbf{k}) = \begin{pmatrix} 0 & \sum_{i=1}^3 t_i e^{-i\mathbf{k} \cdot \tau_i} \\ \sum_{i=1}^3 t_i e^{i\mathbf{k} \cdot \tau_i} & 0 \end{pmatrix}. \quad (2.72)$$

where the subscript “b” means the bulk. $\tau_{i=1,2,3}$ are expressed as $\tau_1 = (0, 1)$, $\tau_2 = (-\frac{\sqrt{3}}{2}, -\frac{1}{2})$, $\tau_3 = (\frac{\sqrt{3}}{2}, -\frac{1}{2})$, and we put the length of the nearest-neighbor bonds as unity. For simplicity t_i are assumed to be positive. The primitive vectors $\mathbf{a}_{i=1,2}$

are $\mathbf{a}_1 = (\frac{\sqrt{3}}{2}, \frac{3}{2})$, $\mathbf{a}_2 = (-\frac{\sqrt{3}}{2}, \frac{3}{2})$, and the reciprocal primitive vectors are $\mathbf{G}_1 = 2\pi\frac{2}{3}(\frac{\sqrt{3}}{2}, \frac{1}{2})$, $\mathbf{G}_2 = 2\pi\frac{2}{3}(-\frac{\sqrt{3}}{2}, \frac{1}{2})$.

We first note that the bulk Hamiltonian H_b has chiral symmetry:

$$\sigma_z H_b \sigma_z = -H_b, \quad (2.73)$$

where σ_z is the Pauli matrix. Therefore, if $|\psi\rangle$ is an eigenstate with an eigenvalue E , $\sigma_z|\psi\rangle$ is an eigenstate with energy $-E$. The eigenvalues are given by

$$E_b(\mathbf{k}) = \pm \left| \sum_{i=1}^3 t_i e^{-i\boldsymbol{\tau}_i \cdot \mathbf{k}} \right|. \quad (2.74)$$

Hereafter we put parameters as $t_2 = t_3 = 1$, and $t_1 = t$, where t is a real positive tunable parameter. The bulk dispersion is given as

$$E_b^2 = \left(t + 2 \cos \frac{\sqrt{3}k_x}{2} \cos \frac{3k_y}{2} \right)^2 + 4 \cos^2 \frac{\sqrt{3}k_x}{2} \sin^2 \frac{3k_y}{2}. \quad (2.75)$$

Because of the chiral symmetry, the gap closes only at zero energy. The bulk gap-closing points (k_x^*, k_y^*) are given by the equations: $\cos \frac{\sqrt{3}k_x^*}{2} = \pm \frac{1}{2}$ and $\sin \frac{3}{2}k_y^* = 0$. The equations give two gap-closing points in the bulk BZ, and they exist for $t \leq 2$. The gap-closing points move with the change of the anisotropy t , as pointed out by Dietl et al. [58]. For $t = 1$, i.e. the tight-binding model of graphene, the upper and lower bands touch at K $(\frac{2\pi\sqrt{3}}{9}, \frac{2\pi}{3})$ and K' $(-\frac{2\pi\sqrt{3}}{9}, \frac{2\pi}{3})$, and with the increase of t the gap-closing points get closer along the line $k_y = \frac{2\pi}{3}$ (Fig. 2.11b). Around each of the two gap-closing points, the dispersion forms a Dirac cone, and Berry phase around each gap-closing point is π , which is protected by chiral symmetry. Because of this π Berry phase, the gap-closing points do not disappear as we change $t (< 2)$. The bulk gap-closing points move in the direction perpendicular to the bonds with anisotropic hopping integral t . At $t = 2$ the two points meet and they annihilate each other at $k_x = 0$ (Fig. 2.11b) [58]. This is possible because the sum of the Berry phase becomes zero, i.e. $\pi + \pi \equiv 0 \pmod{2\pi}$. For $t > 2$, there are no bulk gap-closing points.

The evolution of the edge states with the change of the anisotropy has been studied in several papers [58–60]. As we see in the following, for $t > 2$ flat-band edge states on the zigzag or Klein edges completely cover the BZ, as has been studied by Delplace et al. [59]. For the zigzag edges it occurs when the bond with hopping t is perpendicular to the edge, and for the Klein edges it occurs when the bond with hopping t is not perpendicular to the edge. For these cases with zigzag and Klein edges, dispersions are shown in Fig. 2.11c for $t_1 = 1$ and $t_1 = 2.2$, at $t_2 = t_3 = 1$ in both cases. The flat-band edge states are separated completely from the bulk for $t_1 = 2.2$ (Fig. 2.11c).

To explain this behavior, we solve the Schrödinger equation in the semi-infinite geometry with a zigzag edge. The zigzag edge is assumed to be perpendicular to the bonds with hopping integral t_1 . We express the wavefunction $|\Psi(k)\rangle$ as

$$|\Psi(k)\rangle = \sum_{i=1} (a_i(k)|A_i(k)\rangle + b_i(k)|B_i(k)\rangle), \quad (2.76)$$

where i denotes an index for unit cells containing two sublattice sites, A and B, counted from the edge ($i = 1$), k is the wavenumber along the edge, and $a_i(k)$ ($b_i(k)$) denotes the coefficient for the wavefunctions at A(B) sublattice, $|A_i(k)\rangle$ ($|B_i(k)\rangle$). Acting H onto $|A_i(k)\rangle$ and $|B_i(k)\rangle$, we have

$$\langle B_i(k)|H|A_i(k)\rangle = t_1, \quad (2.77)$$

$$\langle B_{i-1}(k)|H|A_i(k)\rangle = t_2 + t_3 e^{-ik}. \quad (2.78)$$

From Fig. 2.11c, the surface states are expected to be at the zero energy, and as we see later it is the case indeed. When we set the eigenvalue to be zero, $H|\Psi(k)\rangle = 0$, we obtain

$$a_i(t_2 + t_3 e^{-ik}) + a_{i+1}t_1 = 0, \quad b_i = 0. \quad (2.79)$$

Thus the amplitude of the flat-band states is given by

$$a_n(k) = a_1 \left[-\frac{t_2 + t_3 e^{-ik}}{t_1} \right]^{n-1}, \quad b_i = 0 \quad (2.80)$$

where $a_1 = \left[1 - \frac{|t_2 + t_3 e^{-ik}|^2}{t_1^2} \right]^{-1/2}$ from normalization, and the condition for existence of the edge states, i.e. normalizability of the wavefunction, is given as

$$\left| \frac{t_2 + t_3 e^{-ik}}{t_1} \right| < 1. \quad (2.81)$$

For example, for $t_1 = t_2 = t_3$ (graphene model), the wavenumber that satisfies the condition (Eq. 2.81) for existence of the edge state is given as $\frac{2\pi}{3} < k < \frac{4\pi}{3}$, which agrees with the well-known flat band in graphene ribbon with a zigzag edge [55]. In addition, by the relation $\left| \frac{t_2 + t_3 e^{-ik}}{t_1} \right| < \frac{t_2 + t_3}{t_1}$, when $t_1 > t_2 + t_3$ is satisfied, the wavefunction defined by Eq. (2.80) is normalizable for every \mathbf{k} and the flat bands cover the whole 1D BZ. This condition $t_1 > t_2 + t_3$ means that the anisotropy is sufficiently large. These results agree with numerical calculations in Fig. 2.11c.

In Fig. 2.11c we also show results for armchair edges and for Klein (bearded) edges. For armchair edges, there are no flat-band edge states. For Klein edges where

τ_1 -bonds (hopping t_1) are not perpendicular to the edge, there are flat-band edge states; if $t_1 > 2$ the flat-band edge states cover the entire BZ. These results agree with the results by Delplace et al. [59].

2.3.2 Topological Explanation for Existence of the Flat-Band States

In the paper by Ryu and Hatsugai [56], a topological interpretation of the existence of edge states at zero energy in two-dimensional models with chiral symmetry is given. In this section we review this theory by using the tight-binding model on the honeycomb lattice, and show that the flat-band edge states are explained within this theory [56].

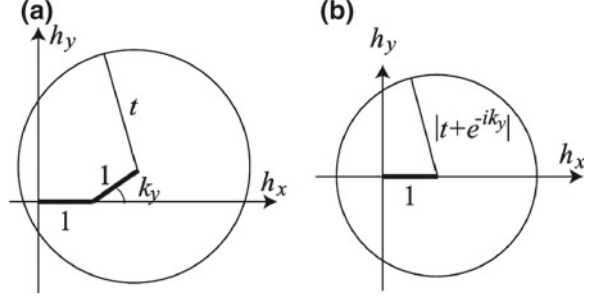
To apply the topological argument by Ryu and Hatsugai [56], the crystal termination is crucial. The way how the edges are oriented and how the crystal is terminated is incorporated into the formalism in the following way. For two-dimensional models with chiral symmetry, for example, we begin with a bulk system, and we cut the system along one direction by cutting the nearest-neighbor bonds, in order to discuss edge states. Let y denote the coordinate along which the system will be cut. Then, following the argument by Ryu and Hatsugai [56], we expand the bulk Hamiltonian by the Pauli matrices σ_x, σ_y as $H = h_x(k'_x, k_y)\sigma_x + h_y(k'_x, k_y)\sigma_y$. Here k_y denotes the component of the wavevector along the y -direction (along the edge), and k'_x is the other component of the wavevector. We note that because we assume chiral symmetry $\sigma_z H \sigma_z = -H$, the 2×2 Hamiltonian H has no σ_z term. Because the bulk system is cut along the y -axis, k'_x will no longer be a good quantum number. Then the criterion by Ryu and Hatsugai [56] says that if the trajectory of (h_x, h_y) for the change of k'_x with fixed k_y encircles the origin, zero-energy edge states exist for the given k_y . If not, zero-energy edge states will not exist [56]. An intuitive picture of this argument is the following. The origin $(h_x, h_y) = (0, 0)$ is a singular point because the bulk Hamiltonian has degenerate eigenvalues at zero energy. Whether the trajectory encircles this singularity or not determines a classification of the Hamiltonian either into a class with no edge state or a class with flat-band edge states. Namely, if the trajectory does not encircle the origin, it can be continuously deformed into a point without encountering the singular point, which leads to an absence of zero-energy boundary states.

We apply this criterion to the present models to show that the flat-band boundary states discussed so far are fully explained by this theory. For the anisotropic honeycomb-lattice models, explanations are given by Delplace et al. [59], and we reproduce it here for illustration. For zigzag edges we have

$$h_x = t \cos(k_y - k'_x) + 1 + \cos k_y, \quad (2.82)$$

$$h_y = -t \sin(k_y - k'_x) + \sin k_y. \quad (2.83)$$

Fig. 2.12 Trajectories of (h_x, h_y) by varying k'_x in (a, b) for the honeycomb-lattice model with zigzag (a), with Klein (b) edges



Hence the trajectory is a circle with a radius $|t|$ centered at $(1 + \cos k_y, \sin k_y)$ (Fig. 2.12a). The condition that it encircles the origin reproduces the range of the wavevector of the flat-band edge states, obtained in the previous section. In particular, for $t > 2$ the trajectory encompasses the origin irrespective of the value of k_y , and existence of the perfectly flat edge band over the whole BZ results, as we discussed previously. The case for the Klein edge is explained similarly, where we have

$$h_x = 1 + \cos(k_y - k'_x) + t \cos k'_x, \quad (2.84)$$

$$h_y = -\sin(k_y - k'_x) + t \sin k'_x. \quad (2.85)$$

with the trajectory shown in Fig. 2.12b. Then it is easily seen that the flat-band edge states extend over the whole BZ when $t > 2$.

2.3.3 Completely Localized Edge States

We have shown that the nearest-neighbor tight-binding models on the honeycomb lattice, have flat-band boundary states covering the whole BZ, when the anisotropy of their hopping integrals is sufficiently large. In general, when systems have completely flat bands over the entire BZ, one can construct a wavefunction which is spatially localized on a finite number of sites. Namely, because of the flatness of the band, any linear combination of the eigenstates within this flat band is also an eigenstate; therefore by taking an appropriate linear combination, one can construct a fully localized state. This is analogous to constructing a spatially localized state as a linear combination of plane waves.

The construction of the fully localized state is possible only when the flat band covers the whole BZ [57]. In this section, we calculate the fully localized wavefunction in the present models. This wavefunction is exponentially decaying in the direction normal to the boundary, while on the outermost atomic layer, the wavefunction is nonzero only on a single site, as schematically shown in Fig. 2.13. We consider semi-infinite systems for the honeycomb lattice with the zigzag edge.

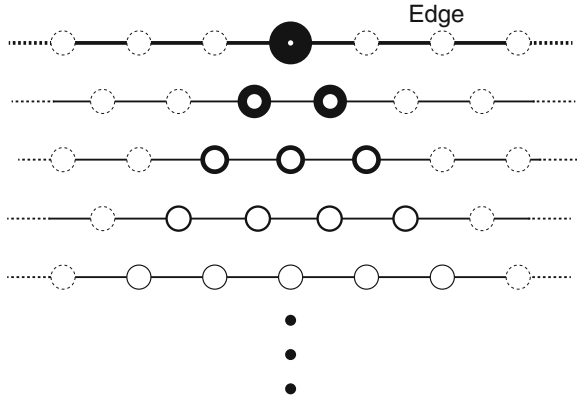


Fig. 2.13 Schematic of spatial distribution of the flat-band surface states. The *circles* are the A sublattice sites, while the amplitudes on B sublattices are zero and are omitted. The *dotted circles* show that their amplitudes of the wavefunction are zero. The *line thickness* of the circle shows the magnitude of the amplitude. The *top* atom has the largest amplitude, and the distribution of the wavefunction spatially spreads toward the interior with exponential decay

Similarly to the previous sections, the outermost atomic layer is assumed to belong to the A sublattice.

We consider the honeycomb lattice in the half plane $y \leq 0$. The zigzag edge is along the x axis, and the origin \mathcal{O} is set to be one site on the zigzag edge. The state at the site $-m\mathbf{a}_1 - n\mathbf{a}_2$ is denoted as $|A_{mn}\rangle$ where $\mathbf{m} = (m, n)$ are nonnegative integers, and $\mathcal{O} = (0, 0)$. We assume that the amplitude of the localized wavefunction on the outermost atomic layer is nonzero only at \mathcal{O} . We express the wavefunction of the localized states as

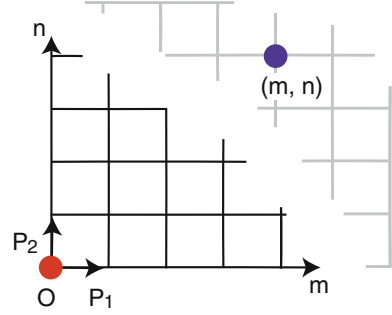
$$|\Psi\rangle = \sum_{m,n} a_{mn} |A_{mn}\rangle, \quad (2.86)$$

where a_{mn} is the amplitude for $|A_{mn}\rangle$ at A sublattice. The amplitude at B sublattice is identically zero. From the Schrödinger equation, we have a relation between amplitudes as

$$a_{mn} = -\frac{t_2}{t_1} a_{m-1n} - \frac{t_3}{t_1} a_{mn-1}. \quad (2.87)$$

Intriguingly, the solution for the above sequence determined by (2.87) is the same as the following problem. Consider a mover in the xy plane on the grid shown in Fig. 2.14. The mover is first on the $\mathcal{O} = (0, 0)$ site. At each step it moves by $(1, 0)$ with a probability P_1 , by $(0, 1)$ with a probability P_2 (Fig. 2.14), and the movement is finished otherwise. Finally after $m+n$ steps the probability P_{mn} that the mover is at (m, n) ($m, n \geq 0$) along the shortest paths is given as

Fig. 2.14 Schematic of the grids for the shortest path problem. The mover is at the origin \mathcal{O} , and it moves along \mathbf{e}_i with the probability P_i , where $(\mathbf{e}_i)_j = \delta_{ij}$



$$P_{mn} = \frac{(m+n)!}{m!n!} P_1^m P_2^n. \quad (2.88)$$

By replacing the probabilities of the movement with the ratio of the hopping integrals,

$$P_i \rightarrow -\frac{t_{i+1}}{t_1}, \quad (2.89)$$

where $i = 1, 2$, we have the amplitude of the wavefunction as

$$a_{mn} = \frac{1}{Z} \frac{(m+n)!}{m!n!} \left(-\frac{t_2}{t_1}\right)^m \left(-\frac{t_3}{t_1}\right)^n \quad (m, n \geq 0), \quad (2.90)$$

where Z is the normalization constant. For $m < 0$ or $n < 0$, a_{mn} vanishes. In this spatial representation of the wavefunction, the condition for existence of the fully localized states on the boundary is that the wavefunction is normalizable. Generally, because $t_{1,2,3}$ are positive, Z satisfies the following relation:

$$\begin{aligned} Z^2 &= \sum_{N=0}^{\infty} \sum_{n,m=0}^N \delta_{n+m,N} P_{mn}^2 \\ &\leq \left(\sum_{N=0}^{\infty} \sum_{n,m=0}^{N=n+m} |P_{mn}| \right)^2 = \left[\sum_{N=0}^{\infty} \left(\frac{t_2 + t_3}{t_1} \right)^N \right]^2. \end{aligned} \quad (2.91)$$

Therefore for $\frac{t_2+t_3}{t_1} < 1$, the normalization constant Z converges; namely the fully localized states appear. This condition is the same as that for the appearance of flat-band edge states.

References

1. K. von Klitzing, K.G. Dorda, M. Pepper, Phys. Rev. Lett. **45**, 494 (1980)
2. M.Z. Hasan, C.L. Kane, Rev. Mod. Phys. **82**, 3045 (2010)
3. R.B. Laughlin, Phys. Rev. B **23**, 5632 (1981)
4. D.J. Thouless, M. Kohmoto, M.P. Nightingale, M. den Nijs, Phys. Rev. Lett. **49**, 405 (1982)
5. M.V. Berry, Proc. R. Soc. Lond. A **392**, 45 (1984)
6. J.E. Avron, D. Osadchy, R. Seiler, Phys. Today **56**, 38 (2003)
7. M. Kohmoto, Ann. Phys. N.Y. **160**, 343 (1985)
8. R.D. King-Smith, D. Vanderbilt, Phys. Rev. B **47**, 1651–1654 (1993)
9. R. Resta, Rev. Mod. Phys. **66**, 899–915 (1994)
10. B.I. Halperin, Phys. Rev. B **25**, 2724 (1982)
11. M. Büttiker, Phys. Rev. B **38**, 9375 (1988)
12. F.D.M. Haldane, Phys. Rev. Lett. **61**, 2015 (1988)
13. C.L. Kane, E.J. Mele, Phys. Rev. Lett. **95**, 226801 (2005)
14. C.L. Kane, E.J. Mele, Phys. Rev. Lett. **95**, 146802 (2005)
15. B.A. Bernevig, T.L. Hughes, S.-C. Zhang, Science **314**, 1757 (2006)
16. J.E. Moore, L. Balents, Phys. Rev. B **75**, 121306(R) (2007)
17. L. Fu, C.L. Kane, E.J. Mele, Phys. Rev. Lett. **98**, 106803 (2007)
18. R. Roy, Phys. Rev. B **79**, 195322 (2009)
19. M. König et al., Science **318**, 766 (2007)
20. R. Roy, Phys. Rev. B **79**, 195321 (2009)
21. D. Hsieh et al., Nature (London) **452**, 970 (2008)
22. Y. Xia et al., Nat. Phys. **5**, 398 (2009)
23. D. Hsieh et al., Nature (London) **460**, 1101 (2009)
24. Y.L. Chen et al., Science **325**, 178 (2009)
25. T. Valla et al., Phys. Rev. B **86**, 241101(R) (2012)
26. C. Xu, J.E. Moore, Phys. Rev. B **73**, 045322 (2006)
27. C. Wu, B.A. Bernevig, S.-C. Zhang, Phys. Rev. Lett. **96**, 106401 (2006)
28. H.J. Goldsmid, *Thermoelectric Refrigeration* (Plenum, New York, 1964)
29. G.A. Slack, in *CRC Handbook of Thermoelectrics* ed by D.M. Rowe (CRC Press, Boca Raton, 1995), pp. 407–440
30. R. Takahashi, S. Murakami, Phys. Rev. B **81**, 161302(R) (2010)
31. P. Ghaemi, R.S.K. Mong, J.E. Moore, Phys. Rev. Lett. **105**, 166603 (2010)
32. L.D. Hicks, M.S. Dresselhaus, Phys. Rev. B **47**, 12727 (1993)
33. L.D. Hicks, M.S. Dresselhaus, Phys. Rev. B **47**, 16631 (1993)
34. R. Takahashi, S. Murakami, Semicond. Sci. Technol. **27**, 124005 (2012)
35. L. Fu, C.L. Kane, Phys. Rev. B **74**, 195312 (2006)
36. S. Murakami, N. Nagaosa, S.-C. Zhang, Science **301**, 1348 (2006)
37. J. Sinova et al., Phys. Rev. Lett. **92**, 126603 (2004)
38. M.I. Dyakanov, V.I. Perel, JETP Lett. **13**, 467 (1971)
39. M.I. Dyakanov, V.I. Perel, Phys. Lett. A **35**, 459 (1971)
40. Y.K. Kato et al., Science **306**, 1910 (2004)
41. J. Wunderlich et al., Phys. Rev. Lett. **94**, 047204 (2005)
42. X.L. Qi et al., Phys. Rev. B **78**, 195424 (2008)
43. Z. Wang et al., New J. Phys. **12**, 065007 (2010)
44. A.M. Essin, J.E. Moore, D. Vanderbilt, Phys. Rev. Lett. **102**, 146805 (2009)
45. L. Fu, C.L. Kane, Phys. Rev. B **76**, 045302 (2007)
46. H. Zhang et al., Nat. Phys. **5**, 438 (2009)
47. C.X. Liu et al., Phys. Rev. B **82**, 045122 (2010)
48. W.-Y. Shan, H.-Z. Lu, S.-Q. Shen, New J. Phys. **12**, 043048 (2010)
49. E.H. Lieb, Phys. Rev. Lett. **62**, 1201 (1989)
50. A. Mielke, J. Phys. A: Math. Gen. **24**, L73 (1991)
51. A. Mielke, J. Phys. A **24**, 3311 (1991)

- 52. A. Mielke, J. Phys. A **25**, 4335 (1992)
- 53. A. Mielke, H. Tasaki, Commun. Math. Phys. **158**, 341 (1993)
- 54. K.S. Novoselov et al., Science **306**, 666 (2004)
- 55. M. Fujita et al., J. Phys. Soc. **65**, 1920 (1996)
- 56. S. Ryu, Y. Hatsugai, Phys. Rev. Lett. **89**, 077002 (2002)
- 57. R. Takahashi, S. Murakami, Phys. Rev. B **88**, 235303 (2013)
- 58. P. Dietl, F. Piechon, G. Montambaux, Phys. Rev. Lett. **100**, 236405 (2008)
- 59. P. Delplace, D. Ullmo, G. Montambaux, Phys. Rev. B **84**, 195452 (2011)
- 60. M. Kohmoto, Y. Hasegawa, Phys. Rev. B **76**, 205402 (2007)

Topological States on Interfaces Protected by
Symmetry

Takahashi, R.

2015, XII, 90 p. 40 illus., 6 illus. in color., Hardcover

ISBN: 978-4-431-55533-9